

Convergent series representation for the generalized oscillator strength of electron-impact ionization and an improved binary-encounter-dipole model

Winifred M. Huo

NASA Ames Research Center, Mail Stop T27B-1, Moffett Field, California 94035-1000

(Received 29 September 2000; revised manuscript received 24 April 2001; published 18 September 2001)

The use of the Bethe cross section in the binary-encounter-dipole (BED) model for electron-impact ionization is studied. While the dipole contribution in the Born approximation accounts for the longest-range interaction in electron-neutral atom/molecule inelastic collisions at any incident energy, the Bethe formula is applicable only at high energies. To derive a suitable representation of the Born cross section for dipole-allowed transitions, a convergent series representation for the generalized oscillator strength (GOS) of electron-impact ionization is studied. It is shown that by transforming to a new variable determined by the location of the singularities of the GOS on the complex plane of momentum transfer K , a series representation for the GOS is obtained that is convergent at all physically attainable values of K . An approximate representation of the GOS that truncates the series representation to the first three terms is also given. The approximate GOS describes the interaction of the electron with a shielded dipole potential and satisfies both Lassetre's limit theorem at $K=0$ and the asymptotic behavior at large K derived by Rau and Fano [A. R. P. Rau and U. Fano, Phys. Rev. **162**, 68 (1967)]. The dipole-Born cross section so obtained is applicable at all incident energies and goes to the Bethe cross section at the high-energy limit. It provides a more suitable representation of the dipole contribution in the BED model than the Bethe cross section and is valid over the entire energy range. A similar analysis of the optical-oscillator strength (OOS) as a function of the complex momentum for the ejected electron k_p , plus the requirement that the OOS satisfies both the low- and high- k_p limits produces an analogous series representation for the OOS. An approximate one-term representation of the OOS is also developed that can be used in modeling calculations. Numerical examples of total ionization cross sections of N_2 , H_2O , CO_2 , CH_4 , and CF_4 using the new analytical representation are presented to illustrate the applicability of the improved BED model.

DOI: 10.1103/PhysRevA.64.042719

PACS number(s): 34.80.Gs, 52.20.Fs

I. INTRODUCTION

Electron-impact ionization of atoms and molecules is a fundamental process in a plasma. While a large experimental database for electron-impact ionization cross sections is available, in a number of cases significant discrepancies still remain. Furthermore, measurements of reactive species such as radicals are known to be difficult. Theoretically, *ab initio* calculation of electron-impact ionization cross sections for atoms is a challenging problem and is actively being pursued [1–4]. In the case of molecules, only Born calculations with a simple function describing the ejected electron have been attempted so far. Thus physically based models are currently the only means to determine the electron-impact ionization cross section of large, complex molecules.

The binary-encounter-dipole (BED) model for electron-impact ionization of Kim and Rudd [5] combines a modified form of the Mott cross section and the Bethe-dipole cross section. In the BED model, the incident-electron energy T appearing in the denominator of the Bethe cross section is replaced by $T + U + \alpha_o^2/2$, with U being the kinetic energy of the bound electron and $\alpha_o^2/2$ its binding energy. Kim and Rudd also introduced a simplified version of the BED model, called the binary-encounter-Bethe (BEB) model in which a simple expression for the optical-oscillator strength, based on the results from H, He, and H_2 , is employed in the expression of the Bethe cross section. Both the BED and BEB models depend only on quantities either determined using

target and ion wave functions or from experiment. Calculations based on either model are generally in good agreement with experiment at incident energies from threshold to several keV. For many cases the deviation from experiment is within 5–15% at the peak, with the BED model performing somewhat better than the BEB model [6–10]. More recently, Khare *et al.* [11,12] introduced their version of the binary-encounter-dipole model. Again the Bethe cross section was used to describe long-range dipole collisions.

While the BED/BEB model has met much success, puzzling aspects of the model exist. The Bethe cross section is a high-energy approximation. However, the BED and BEB models have been applied successfully at energies close to the first ionization threshold. Furthermore, analysis of the calculated cross sections shows that the contribution of the Bethe term at low energies is nontrivial, as much as 30–50% of the total cross section. Does the success of the BED/BEB model arise from the empirical replacement of $1/T$ by $1/(T + U + \alpha_o^2/2)$ in the Bethe cross section? If so, what is the theoretical basis for doing so? Another puzzling aspect is the manner in which BED/BEB cross sections vary with improved molecular parameters. In a BEB calculation of perfluorocarbons [9], BEB cross sections for CF_4 agree best with experiment when RHF parameters are used. But for C_2F_6 and C_3F_8 , parameters from complete-active-space self-consistent-field (CASSCF) calculations give the best results. There is no obvious explanation to account for such irregular behavior. In order to put the BED/BEB model on a

sound theoretical footing, it is important to investigate this further.

Theoretically, the most questionable aspect of the BED/BEB model lies in the use of the Bethe cross section at low incident-electron energies. The role of the dipole interaction (or transition-dipole interaction for inelastic collisions) in the Born series has been studied previously by Huo [13]. By analyzing the Fourier transform of the collision amplitude, including both Born and non-Born contributions, it was demonstrated that the long-range dipole-interaction potential $1/r^2$, coming from the Born term, is the longest-range potential in electron-neutral atom/molecule inelastic collisions. All non-Born contributions are of shorter range. It was also argued that the long-range dipole potential in the Born term must be shielded as the incident electron moves into the molecular-charge cloud [14]. These results hold independent of the incident-electron energy. It can therefore be argued that, in order to account for dipole interactions over a wide energy range, the Born cross section, instead of the Bethe cross section, is a more appropriate form to use.

To derive a simple, analytical representation of the Born cross section, we study the generalized oscillator strength (GOS) for electron-impact ionization. GOS is frequently employed in the study of high-energy electron collisions [15]. However, certain properties of the GOS are actually applicable to low-energy collisions as well. One example is Lassetre's limit theorem [16,17] which states that at the limit of zero-momentum transfer, $K=0$, the GOS is equal to the optical-oscillator strength. This result holds for any atoms or molecule regardless of whether the Born approximation is applicable. While zero-momentum transfer for inelastic collisions is a mathematical limit reachable only by extrapolation from the measured GOS, the limit theorem shows that extrapolation can be done using low as well as high-energy data.

For inelastic collisions involving bound-bound transitions, Lassetre also investigated a convergent series representation of the GOS [18]. An expansion of the GOS in a power series of K generally leads to a series with finite radius of convergence. However, by introducing a new expansion variable $t = K^2/(K^2 + \alpha^2)$, based on the location of the singularities of the GOS as a function of complex K , Lassetre showed that it is possible to transform the GOS representation to a new series that converges for all physically attainable values of K . Here $K = \pm i\alpha$ is the position of the singularities for the GOS, and $\alpha^2 = \alpha_1^2 + \alpha_2^2$, with $\alpha_i^2 = -2\mathcal{E}_i$ and \mathcal{E}_i the binding energy of the electron being excited.

In applying Lassetre's series to deduce the limit of GOS at $K=0$, Huo [19] showed that at the limit of zero K the derivative of the GOS with respect to K does not vanish and the derivative with respect to K^2 becomes infinite at all finite incident energies, both resulting from the non-Born contributions. Thus it is necessary to include odd-power terms in K in a series expansion of the GOS to deduce its limit at $K=0$. Recently Felfli *et al.* [20] introduced a new generalized Lassetre expansion that employed a Reggie Pole representation for the non-Born term and demonstrated reliable extrapolation to the OOS limit even at low incident-electron energies.

While Lassetre's series is often useful in fitting experi-

mental and theoretical data for bound-bound transitions, a similar analysis for electron-impact ionization has not been carried out. Thus the study of ionization GOS does not have the benefit of the convergent series expansion available for bound-bound transitions. To derive a simple, analytical representation of the Born cross section for ionization, we employ Lassetre's approach and analyze the singularities of the GOS as a function of complex K . A convergent series representation of the GOS for electron-impact ionization is derived by transforming to a new variable that accounts for the singularities. The resulting series bears a strong resemblance to Lassetre's result for bound-bound transitions except that the momentum of the ejected electron is involved. By retaining the first term in this series, and requiring this representation to satisfy both the Lassetre's limit theorem as $K \rightarrow 0$ and the correct asymptotic behavior at large K derived by Rau and Fano [21], we obtain a simple analytic form for the GOS for dipole-allowed ionization. A three-term representation of the GOS is also proposed. Both are suitable for modeling purposes. The latter, however, provides a better description of the shielding of the dipole potential.

Alternatively, numerical calculations of the Born cross section for electron-impact ionization of atoms and molecules can be used directly in the BED model. Unless a Coulomb wave function is used for the ejected electron, these calculations are quite involved, particularly so when the result must be integrated over the momentum transfer of the incoming electron and the energy of the ejected electron. We consider the present approach, employing a simple representation of the Born cross section with parameters obtainable by bound-state quantum-chemistry calculations of the target and ions or tabulated thermochemistry data, to be more efficient. In this sense, the present approach retains much of the utility of the original BED/BEB model and requires a relatively small amount of computing effort.

An analogous complex analysis for the optical-oscillator strength (OOS) for dipole-allowed ionization has also been carried out. Based on its singularities on the complex momentum plane for the ejected electron, and the limiting behavior of the OOS at large and small ejected-electron momentum k_p , we arrive at a series representation of the OOS. An approximate one-term expression is also developed for modeling purposes. This expression is different from what is used by Kim and Rudd [5] in their BEB approximation.

By combining the dipole-Born cross section and the symmetrized Mott cross section, with the incident-electron energy modified using the binary-encounter model, we obtain an improved BED (iBED) model. Further simplification by employing the one-term representation of the OOS gives the simplified version of the iBED (siBED) model. Numerical calculations of N_2 , H_2O , CO_2 , CH_4 , and CF_4 using iBED/siBED demonstrate the applicability of these models.

Theoretical developments are presented in Sec. II and numerical examples in Sec. III. Sec. IV summarizes our results.

II. THEORETICAL DEVELOPMENT

The generalized oscillator strength f_{Jpo} for electron-impact ionization of an atom or molecule from the initial state o to

the final state with the ion at state p and the ejected electron with energy E_p and momentum k_p is defined by

$$f_{po}(K, E_p) = \frac{1}{2} W_{po} K^2 \frac{k_o}{k_f} \frac{d^2 \sigma}{dE_p d\Omega}, \quad (2.1)$$

where $d^2 \sigma / dE_p d\Omega$ is the differential cross section, k_o and k_f the momenta of the incident and scattered electron, K the momentum transfer, and W_{po} the excitation energy. For ionization W_{po} is the energy difference between the initial neutral state and the p th ion state plus the ejected-electron energy. In the Born approximation f_{po} is given by

$$f_{po}(K, E_p) = \frac{2 W_{po}}{K^2} |\varepsilon_{po}(K, E_p)|^2. \quad (2.2)$$

The form factor ε_{po} is given by

$$\varepsilon_{po}(K, E_p) = \left\langle \Psi_p(\tau_1 \cdots \tau_n, \mathbf{R}) \left| \sum_{i=1}^n e^{i\mathbf{K} \cdot \mathbf{r}_i} \Psi_o(\tau_1 \cdots \tau_n, \mathbf{R}) \right. \right\rangle. \quad (2.3)$$

Here τ_i is the i th electron coordinate including spin and \mathbf{R} the totality of the nuclear coordinates. The final-state wave function $\Psi_p(\tau_1 \cdots \tau_n, \mathbf{R})$ is approximated by an antisymmetrized product of the ion wave function $\Phi_p(\tau_2 \cdots \tau_n, \mathbf{R})$ and the continuum wave function for the ejected electron $\varphi_p(\tau_1, \mathbf{R})$ (See discussions near the end of Sec. II A for the removal of this approximation). Due to the large difference between the electronic and nuclear mass, the ionization of an electron is significantly faster than the relaxation of the nuclear configuration and the sudden approximation can be employed. In that case ε_{po} is rewritten as

$$\varepsilon_{po}(K, E_p) = \left\langle \Psi_p(\tau_1 \cdots \tau_n, \mathbf{R}_o) \left| \sum_{i=1}^n e^{i\mathbf{K} \cdot \mathbf{r}_i} \Psi_o(\tau_1 \cdots \tau_n, \mathbf{R}_o) \right. \right\rangle \times \langle \zeta_p(\mathbf{R}) | \zeta_o(\mathbf{R}) \rangle, \quad (2.4)$$

where \mathbf{R}_o is the equilibrium geometry of the initial state and ζ the nuclear wave function. It should be pointed out that the results presented below do not depend on the validity of the sudden approximation. However, in the sudden approximation ε_{po} is expressed in terms of a product of electronic and nuclear matrix elements and the derivation is more transparent. In the following, we shall omit writing out the nuclear-overlap term and the nuclear geometry \mathbf{R}_o .

In Sec. II A the location of the singularities for the GOS are derived with the assumption that the initial- and final-state electronic wave functions are one-electron orthogonal [22] to each other at any nuclear configuration. The assumption of one-electron orthogonality further simplifies the expression for ε_{po} to

$$\varepsilon_{po}(K, E_p) = \langle \varphi_p(\mathbf{r}) | e^{i\mathbf{K} \cdot \mathbf{r}} | \varphi_o(\mathbf{r}) \rangle. \quad (2.5)$$

Again the assumption of one-electron orthogonality is not essential to our results but makes the presentation simpler. The relaxation of the sudden approximation, one-electron orthogonality, and the simple product form of the final-state wave function will be discussed in Sec. II A.

The present study considers only the Born contribution to the GOS. Our analysis determines the primary singularities in the GOS and is sufficient for the derivation of a convergent series representation of the Born cross section, one of the goals of this paper. Additional singularities in the GOS may arise from the non-Born contributions but they will not be considered here.

A. Singularities of the GOS on the complex K plane

The rationale for deriving a series representation of the GOS based on its singularities comes from Liouville's theorem, which states that a function $f(z)$ that is analytic for all values of z and bounded as $|z| \rightarrow \infty$ must be a constant. Thus it follows that we can determine the GOS to an additive constant if all its singularities are known. The present analysis is an extension of Lassette's work on the GOS for bound-bound transitions.

The wave functions $\varphi_o(\mathbf{r})$ and $\varphi_p(\mathbf{r})$ are expanded in terms of spherical harmonics,

$$\varphi_i(\mathbf{r}) = \sum_{l_i m_i} r^{-1} R_{l_i m_i}(r) Y_{l_i m_i}(\hat{r}), \quad (2.6)$$

with the subscript i representing either o or p . After a similar spherical-harmonics expansion for $e^{i\mathbf{K} \cdot \mathbf{r}}$ and integrations over the angular variables, ε_{po} can be written as

$$\varepsilon_{po}(K, E_p) = \sum_{\lambda_o \mu_o} \sum_{\lambda_p \mu_p} \sum_{\lambda \mu} a \times \int_0^\infty R_{p \lambda \mu_p}^*(r) j_\lambda(Kr) R_{o \lambda_o \mu_o}(r) dr. \quad (2.7)$$

Here the summations over $\lambda, \mu, \lambda_o, \mu_o, \lambda_p,$ and μ_p cover the allowed values of $l, m, l_o, m_o, l_p,$ and m_p after angular integrations. The constant $a = a(\lambda_o \mu_o \lambda_p \mu_p \lambda \mu)$ comes from the angular integration. The radial integral is separated into two regions: the first, $\varepsilon^{(i)}$, is inside a sphere with a large radius C , and the second, $\varepsilon^{(e)}$, outside this sphere. By expanding the Bessel function $j_\lambda(Kr)$ in an ascending series of Kr , it is seen immediately that for any finite value of K , $\varepsilon^{(i)}$ is regular. Thus any singularity of ε must come from the exterior integral $\varepsilon^{(e)}$ that is given by

$$\varepsilon^{(e)} = \sum_{\lambda_o \mu_o} \sum_{\lambda_p \mu_p} \sum_{\lambda \mu} a \int_C^\infty R_{p \lambda \mu_p}^*(r) \times \frac{\sin(Kr - \lambda \pi/2)}{Kr} R_{o \lambda_o \mu_o}(r) dr. \quad (2.8)$$

Since $\sin(Kr - \lambda \pi/2)/Kr$ is an analytic function of both K and r near $K=0$, $\varepsilon^{(e)}$ has no singularities at $K=0$.

If the radius of the sphere C is chosen to be so large that exchange and correlation effects are unimportant outside, the asymptotic form of $R_{o\lambda_o\mu_o}(r)$ satisfies the differential equation,

$$\frac{d^2}{dr^2}R_{o\lambda_o\mu_o}(r) + \left[2\mathcal{E}_o + \frac{2}{r} - \frac{\lambda_o(\lambda_o+1)}{r^2} \right] R_{o\lambda_o\mu_o}(r) = 0, \quad (2.9)$$

$r \geq C$

where \mathcal{E}_o is the binding energy of the electron. Thus the leading term of $R_{o\lambda_o\mu_o}$ in the asymptotic expansion at large r has the form,

$$\lim_{r \geq C} R_{o\lambda_o\mu_o}(r) \approx b_o r^{1/\alpha_o} e^{-\alpha_o r}, \quad (2.10)$$

with $\alpha_o = \sqrt{-2\mathcal{E}_o}$ and b_o a normalization constant.

Asymptotically, the ejected electron behaves like a Coulomb wave,

$$\begin{aligned} \lim_{r \geq C} R_{p\lambda_p\mu_p}(r) &= b_1 (k_p r)^{-i\gamma} \exp[i(k_p r - \lambda_p \pi/2 + \eta_p)] \\ &+ b_2 (k_p r)^{i\gamma} \exp[-i(k_p r - \lambda_p \pi/2 + \eta_p)], \end{aligned} \quad (2.11)$$

with $\eta_p = \arg \Gamma(\lambda_p + 1 + i\gamma)$ and $\gamma = -1/k_p$.

Using Eqs. (2.10) and (2.11), $\varepsilon^{(e)}$ can be rewritten as

$$\begin{aligned} K\varepsilon^{(e)} &= a_1 \int_C^\infty r^{1/\alpha_o - i\gamma - 1} \exp\{[i(K + k_p) - \alpha_o]r\} dr \\ &+ a_2 \int_C^\infty r^{1/\alpha_o + i\gamma - 1} \exp\{[i(K - k_p) - \alpha_o]r\} dr \\ &+ a_3 \int_C^\infty r^{1/\alpha_o - i\gamma - 1} \exp\{[-i(K - k_p) - \alpha_o]r\} dr \\ &+ a_4 \int_C^\infty r^{1/\alpha_o + i\gamma - 1} \exp\{[-i(K + k_p) - \alpha_o]r\} dr. \end{aligned} \quad (2.12)$$

Let us consider the first integral in Eq. (2.12),

$$I_1 = \int_C^\infty r^\beta e^{(z - \alpha_o)r} dr, \quad (2.13)$$

with $\beta = 1/\alpha_o - i\gamma - 1$ and $z = i(K + k_p)$. It can be readily shown that I_1 satisfies the following differential equation:

$$\frac{d^2 I_1}{dz^2} + \left(\frac{\beta + 2}{z - \alpha_o} - C \right) \frac{dI_1}{dz} - \frac{C(\beta + 1)}{z - \alpha_o} I_1 = 0. \quad (2.14)$$

The differential equation (2.14) is linear and homogeneous. Hence the only singularities of I_1 are located at the points for which the coefficients are singular. These points are at z

$= \alpha_o$ and $z = \infty$. The singular point at $z = \alpha_o$ is regular. To determine if it is a branch cut off a pole, we use the following series expansion for I_1 ,

$$I_1 = (z - \alpha_o)^s \sum_{n=0}^{\infty} \xi_n (z - \alpha_o)^n. \quad (2.15)$$

At $z = \alpha_o$, the only nonvanishing term is $\xi_o (z - \alpha_o)^s$. Substitute the expression of I_1 to Eq. (2.14), we find

$$\begin{aligned} [s(s-1) + s(\beta+2)](z - \alpha_o)^{s-2} \\ - C[s + (\beta+1)](z - \alpha_o)^{s-1} = 0. \end{aligned} \quad (2.16)$$

The indicial equation for the $(z - \alpha_o)^{s-2}$ term is

$$s(s-1) + (\beta+2)s = 0. \quad (2.17)$$

For the $(z - \alpha_o)^{s-1}$ term it is

$$s + (\beta+1) = 0. \quad (2.18)$$

The solution of Eq. (2.17) is $s=0$ and $s = -(\beta+1)$, and for Eq. (2.18) it is $s = -(\beta+1)$. The solution $s=0$ gives rise to an analytic function of I_1 and thus is of no interest. The solution $s = -(\beta+1)$ identifies the singularity at $z = \alpha_o$ to be a branch point if β is a noninteger or a pole of order $\beta + 1$ if β is an integer.

Similar analysis can be applied to the other three integrals in Eq. (2.12). Thus the form factor ε_{p_o} has singularities at the following locations:

$$\begin{aligned} K &= \pm k_p - i\alpha_o, \\ K &= \pm k_p + i\alpha_o. \end{aligned} \quad (2.19)$$

In addition, ε_{p_o} may also be singular at $K = \infty$, but this value of K is not physically reachable.

Based on Eq. (2.2) f_{p_o} will have the same set of singularities as ε_{p_o} , i.e., the points listed in Eq. (2.19). In addition, it may also be singular at $K=0$ and $K=\infty$. However, Lassettre's limit theorem [16,17] states that,

$$\lim_{K \rightarrow 0} f_{p_o}(K, E_p) \rightarrow f_{p_o}^{(o)}(E_p), \quad (2.20)$$

with $f_{p_o}^{(o)}(E_p)$ the optical-oscillator strength. Since $f_{p_o}^{(o)}(E_p)$ is a constant, $f_{p_o}(K, E_p)$ should also be regular at $K=0$. Otherwise Lassettre's limit theorem will not hold. On the other hand, $f_{p_o}(K, E_p)$, like ε_{p_o} , may be singular at $K=\infty$. This singularity is not considered here because $K=\infty$ is not physically accessible.

It is important to point out that we have located the singularities for $f_{p_o}(K, E_p)$ based on the asymptotic forms of the initial and final wave functions. Equations (2.10) and (2.11) are accurate representations of $R_{o\lambda_o\mu_o}$ and $R_{p\lambda_p\mu_p}$ at $r \geq C$. No approximation has been assumed for the full-range wave function φ_o or φ_p . In particular, since asymptotically $R_{o\lambda_o\mu_o}$ and $R_{p\lambda_p\mu_p}$ can be represented by single-center wave functions, their multicenter nature in the interior region does not enter into the derivation of the singularities. Also, while

the Bethe cross section uses a Coulomb wave to represent the ejected electron, we only require that the ejected-electron wave function asymptotically behaves like a Coulomb wave.

Similarly, the removal of the sudden approximation for nuclear motion and the assumption of one-electron orthogonality for initial and final wave functions will not invalidate the present result. If the Born-Oppenheimer approximation is used instead of the sudden approximation, ε_{po} is given by

$$\varepsilon_{po}(K, E_p) = \int \zeta_p^*(\mathbf{R}) \left\langle \Psi_p(\tau_1 \cdots \tau_n, \mathbf{R}) \right| \times \sum_{i=1}^n e^{i\mathbf{k} \cdot \mathbf{r}_i} \left| \Psi_o(\tau_1 \cdots \tau_n, \mathbf{R}) \right\rangle \zeta_o(\mathbf{R}) d\mathbf{R}, \quad (2.21)$$

instead of Eq. (2.4). The $\langle \rangle$ in the integrand denotes an integration over all electronic coordinates. The fact that the radial integral $\varepsilon^{(e)}$ is now \mathbf{R} dependent does not change the nature of the singularity. However, α_o and k_p need to be averaged over the nuclear wave functions. This leads to the use of the electron-binding energy \mathcal{E}_o for a particular rovibrational level of the initial state and the ejected-electron energy E_p associated with a particular rovibrational level of the ion.

The relaxation of the one-electron orthogonality also will not change the major conclusions. If the initial and final states are not one-electron orthogonal, the expression for ε_{po} will include overlap integrals and possible additional singularities coming from the non-orthogonal orbitals. Nevertheless, the singularities identified in Eq. (2.19) are still the primary singular points (or branch cuts).

The removal of the approximation that the final-state wave function be represented by an antisymmetrized product of the ion wave function and ejected-electron wave function also will not alter the results on the singularities. A more accurate representation of the final-state wave function is obtained by a linear combination of such products. The additional terms, which describe the correlation between the ejected electron and the bound electrons of the ion, go to zero asymptotically as $r \rightarrow \infty$. Thus we can choose the radius C that partitions the inner and outer integrals, $\varepsilon^{(i)}$ and $\varepsilon^{(e)}$, to be so large that at C those terms become negligible compared to the term associated with the outgoing Coulomb wave. Thus we conclude that the same set of singularities will result using a more sophisticated final-state wave function.

For bound-bound transitions, Lassette [18] derived the following singularities for the GOS:

$$K = \pm i(\alpha_o + \alpha_b). \quad (2.22)$$

Here $\alpha_b = \sqrt{-2\mathcal{E}_b}$ and \mathcal{E}_b is the binding energy of the excited-state electron. Notice that for both bound-bound transitions and ionization, the location of the singularities in the GOS depends only on energies, and not on l_o, m_o, l_p, m_p, l , and m .

To test the validity of Eq. (2.19), we compare our result with the generalized oscillator strength for electron-impact ionization of H atom originally derived by Bethe [17] and by Massey and Mohr [23],

$$f(K, E_p) = \frac{2^8 [K^2 + (k_p^2 + \alpha_o^2)/3] (k_p^2 + \alpha_o^2)}{[(K + k_p)^2 + \alpha_o^2]^3 [(K - k_p)^2 + \alpha_o^2]^3} \times [1 - \exp(-2\pi/k_p)]^{-1} \times \exp\left\{-\frac{2}{k_p} \arctan\left[\frac{2k_p}{K^2 - k_p^2 + \alpha_o^2}\right]\right\}. \quad (2.23)$$

Walske [24] and Holt [25] pointed out that the derivation of Eq. (2.23) requires the branch lying between 0 and π to be used for the multivalued arctangent function. Taking this into account, the location of the singularities of the H-atom GOS are identical with the list in Eq. (2.19).

Based on Eq. (2.19), a series representation for f_{po} that converges for all physically accessible values of K can be constructed. A general form will be,

$$f_{po}(K, E_p) = [(K + k_p)^2 + \alpha_o^2]^{s_1} \times [(K - k_p)^2 + \alpha_o^2]^{s_2} \sum_{n_1=0}^{\infty} \sum_{n_2=0}^{\infty} \xi_{n_1 n_2} \times \frac{K^{2(n_1+n_2)}}{[(K + k_p)^2 + \alpha_o^2]^{n_1} [(K - k_p)^2 + \alpha_o^2]^{n_2}}. \quad (2.24)$$

As far as we know, this is the first derivation of a series representation of $f_{po}(K, E_p)$ based on its singularities on the complex K plane. As in Lassette's series for bound-bound transitions, this series should converge for all physically accessible values of K . Inokuti *et al.* [26] studied the analytical properties of the GOS df_{po}/dE_p , i.e., the integral of $f_{po}(K, E_p)$ over K . They proposed to fit the GOS by a power series of $E_p/\Delta E$, with ΔE the energy transfer. However, their approach appeared to work well only at high energies.

Equation (2.24) is applicable to any type of electron-impact ionization, including dipole- or quadrupole-allowed or symmetry-forbidden transitions. In Sec. II B an approximate representation of the GOS for dipole-allowed ionization will be derived.

B. GOS for dipole-allowed ionization and its approximate expression

Using the alternate expression of the form factor

$$\varepsilon_{po}(K, E_p) = \left\langle \Psi_p(\tau_1 \cdots \tau_n, \mathbf{R}) e^{i\mathbf{k}_f \cdot \mathbf{r}_o} \right| \sum_i \frac{1}{|\mathbf{r}_o - \mathbf{r}_i|} - \sum_s \frac{Z_s}{|\mathbf{r}_o - \mathbf{R}_s|} \left| \Psi_o(\tau_1 \cdots \tau_n, \mathbf{R}) e^{i\mathbf{k}_o \cdot \mathbf{r}_o} \right\rangle, \quad (2.25)$$

it is readily seen that ϵ_{p_o} , and hence f_{p_o} , includes ionization of all symmetry types. However, only the dipole-Bethe contribution is used in the BED model. Furthermore, while the expansion of f_{p_o} in Eq. (2.24) is useful for analyzing experimental data, it is unsuited for simple-model calculations such as the BED calculations. For that purpose, a simpler expression is preferable with the expansion coefficient determined by known physical conditions that the GOS must satisfy. Two physical conditions are used. The first is Lassette's limit theorem, which determines the value of the GOS at the limit $K=0$. The second is the asymptotic behavior of the GOS at large K . Rau and Fano [21] showed that for dipole-allowed transitions, the GOS should decrease as K^{-12} at large K . Thus for dipole-allowed transitions, a one-term expression for f_{p_o} that accounts for the singularities listed in Eq. (2.19) and satisfies both physical conditions listed above is

$$\hat{f}_{p_o}(K, E_p) = \frac{df_{p_o}^{(0)}(E_p)}{dE_p} \frac{(k_p^2 + \alpha_o^2)^6}{[(K+k_p)^2 + \alpha_o^2]^3 [(K-k_p)^2 + \alpha_o^2]^3}. \quad (2.26)$$

Here \hat{f}_{p_o} denotes the dipole GOS, to be distinguished from the GOS f_{p_o} that includes transitions of all symmetry types. Also, the OOS $f_{p_o}^{(o)}$ is written out explicitly as a differential with respect to the ejected-electron energy. Comparing Eq. (2.26) with Eq. (2.23), we find that the GOS for H-atom ionization has two contributions, one that does not vanish at $K=0$ and decreases as K^{-12} at large K , and the second that vanishes at $K=0$ and decreases as K^{-10} at large K . The first comes from a dipole transition and the second a nondipole transition. The GOS in Eq. (2.26), on the other hand, only accounts for the dipole contribution. Also Eq. (2.26) includes only the Born contribution to the GOS. Consequently the expansion only includes even powers of K . If non-Born contributions are included, Eq. (2.26) needs to be modified to include odd-power K terms.

Note that Lassette's limit theorem uniquely defines the functional dependence of f_{p_o} and its magnitude at $K=0$. On the other hand, Rau and Fano's large- K limit only provides the functional dependence at large K , but not its magnitude. Thus the one-term expression in Eq. (2.26) describes the small- K behavior of f_{p_o} better than large K . An analogous situation occurs in Lassette's series representation for the GOS of bound-bound transitions. In fitting experimental data for bound-bound transitions, it has been found that more than one term in the expansion is necessary to give a good description of f over a wide range of K . In the present case, a corresponding three-term expression is given by

$$\hat{f}_{p_o}(K, E_p) = \frac{df_{p_o}^{(0)}(E_p)}{dE_p} \frac{(k_p^2 + \alpha_o^2)^6}{[(K+k_p)^2 + \alpha_o^2]^3 [(K-k_p)^2 + \alpha_o^2]^3} \times \{1 + d_1 t + d_2 t^2\}, \quad (2.27)$$

with

$$t = \frac{K^4}{[(K+k_p)^2 + \alpha_o^2][(K-k_p)^2 + \alpha_o^2]}. \quad (2.28)$$

The values of d_1 and d_2 can be obtained using experimental or theoretical differential cross-section data at large K . In the absence of such data, they can be determined based on fitting integrated cross sections.

To understand what roles the three terms in Eq. (2.27) play, let us consider the spherical-harmonics expansion of the Coulomb potential,

$$\frac{1}{|\mathbf{r}_o - \mathbf{r}_i|} = \sum_{\ell=0}^{\infty} \sum_{m=-\ell}^{\ell} \frac{4\pi}{2\ell+1} \frac{r_{<}^{\ell}}{r_{>}^{\ell+1}} Y_{\ell m}^*(\hat{r}_o) Y_{\ell m}(\hat{r}_i), \quad (2.29)$$

where $r_{<} = (r_o, r_i)_{\min}$ and $r_{>} = (r_o, r_i)_{\max}$. For dipole interaction, $\ell = 1$,

$$V_{dipole} = \sum_{m=-1}^1 \frac{4\pi}{3} \frac{r_{<}}{r_{>}^2} Y_{1m}^*(\hat{r}_o) Y_{1m}(\hat{r}_i).$$

The first term in \hat{f}_{p_o} , which becomes the OOS at $K=0$ and hence proportional to the transition dipole moment, can be identified with the long-range dipole interaction for $r_o > r_i$. The second and third terms in Eq. (2.27), which vanish at $K=0$, can be considered as contributions from the short-range part of a shielded dipole potential. This is consistent with the fact that the second and third terms become more important with increasing K since large-angle scattering samples close scattering more. The shielding also becomes more important as the incident-electron energy increases from threshold because it is more difficult for low-energy electrons to come close. The fact that the shielding terms become more important at higher energies distinguishes it from a polarization potential, which is most important at low energies.

C. The dipole Born cross section and its high-energy limit

Using the GOS in Eq. (2.27), the singly differential Born cross section is written as

$$\begin{aligned} \frac{d\sigma_{p_o}(E_p)}{dE_p} &= \frac{4\pi}{k_o^2 W_{p_o}} \frac{df_{p_o}^{(o)}(E_p)}{dE_p} (k_p^2 + \alpha_o^2)^6 \\ &\times \int_{K_{\min}}^{K_{\max}} \frac{1 + d_1 t + d_2 t^2}{K[(K+k_p)^2 + \alpha_o^2]^3 [(K-k_p)^2 + \alpha_o^2]^3} dK. \end{aligned} \quad (2.30)$$

One test for the validity of the approximate Born cross section so obtained is to see if it reaches the Bethe asymptote as $T \rightarrow \infty$, with $T = k_o^2/2$. To analyze the high-energy behavior of the approximate Born cross section, we follow the procedure described in Ref. [15], Sec. 4.1 and 4.3, and find

$$\lim_{T \rightarrow \infty} \sigma_{po} = \frac{\pi \ln(T)}{T} \int_0^\infty \frac{1}{E_p + \alpha_o/2} \frac{df_{po}^{(o)}(E_p)}{dE_p} dE_p + O(T^0). \quad (2.31)$$

Similarly, the high-energy limit of the stopping cross section is

$$\lim_{T \rightarrow \infty} \sigma_{po}^{ST} = 2 \int_0^\infty W_{po} \frac{d\sigma_{po}(E_p)}{dE_p} dE_p = 2\pi N_i \frac{\ln(T)}{T}. \quad (2.32)$$

with

$$N_i = \int_0^\infty \frac{df_{po}^{(o)}}{dE_p} dE_p. \quad (2.33)$$

Thus σ_{po} and σ_{po}^{ST} are identical with their respective Bethe asymptotes. For nondipole allowed transitions, the Bethe asymptotes for the integrated and stopping cross sections has $1/T$ instead of $\ln T/T$ dependence [15]. Thus as $T \rightarrow \infty$ Eqs. (2.31) and (2.32) are the sole contributors to the Bethe asymptotes for the $o \rightarrow p$ ionization processes.

D. Singularities of the optical-oscillator strength on the complex k_p plane

1. Singularities of $f_{po}^{(o)}$

The analysis in Sec. II A can be employed to analyze the optical-oscillator strength,

$$\frac{df_{po}^{(o)}}{dE_p} = 2W_{po} |M_{po}|^2, \quad (2.34)$$

$$M_{po} = \langle \varphi_p(\mathbf{r}) | \mathbf{r} | \varphi_o(\mathbf{r}) \rangle. \quad (2.35)$$

Again the singularities of M_{po} are located in the radial integral outside a large sphere with radius C . The outer integrals are,

$$I_+ = \int_C^\infty r^{1/\alpha_o - i\gamma + 1} e^{(ik_p - \alpha_o)r} dr, \quad (2.36)$$

$$I_- = \int_C^\infty r^{1/\alpha_o + i\gamma + 1} e^{(-ik_p - \alpha_o)r} dr.$$

The singularities are located at $k_p = \pm i\alpha_o$. A convergent series representation of $f_{po}^{(o)}$ for all physically accessible values of k_p can be obtained using the transformed variable q ,

$$q = \frac{k_p^2}{k_p^2 + \alpha_o^2}. \quad (2.37)$$

2. A series representation for $f_{po}^{(o)}$

To derive a series representation for $f_{po}^{(o)}$, we make use of the asymptotic behavior of M_{po} at small and large k_p . At the limit of zero k_p , M_{po} should match smoothly with the bound-bound transition moment. The large k_p behavior of

M_{po} has been investigated by Rau and Fano [21] using an energy-normalized spherical Bessel function to represent $\varphi_p(\mathbf{r})$. They obtained a $k_p^{-(\lambda_o + \lambda_p + 2.5)}$ dependence for M_{po} . Since the minimum value of $\lambda_o + \lambda_p$ is 1, M_{po} varies at least as $k_p^{-3.5}$ at large k_p . However, if $\lambda_p = \lambda_o + 1$, the $k_p^{-3.5}$ term vanishes and M_{po} varies at least like $k_p^{-4.5}$. Based on the two asymptotic limits and the relationship $2W_{po} = k_p^2 + \alpha_o^2$, the following series is recommended,

$$\frac{df_{po}^{(o)}}{dE_p} = \frac{1}{(k_p^2 + \alpha_o^2)^4} \left\{ a_0 + k_p \sum_{n=0}^{\infty} c_n \left(\frac{k_p^2}{k_p^2 + \alpha_o^2} \right)^n \right\}. \quad (2.38)$$

There are other, alternate series representations that account for the singularities on the complex k_p plane and satisfy all the necessary constraints. For example,

$$\frac{df_{po}^{(o)}}{dE_p} = \frac{1}{(k_p^2 + \alpha_o^2)^{7/2}} \sum_{n=0}^{\infty} c_n \left(\frac{k_p^2}{k_p^2 + \alpha_o^2} \right)^n. \quad (2.39)$$

In Eq. (2.38) the singularities at $k_p = \pm i\alpha_o$ are represented as poles whereas in Eq. (2.39) they are presented as branch points. Based on our experience in fitting the OOS for a number of ionization channels of N_2 and CH_4 , Eq. (2.38) generally converges faster than Eq. (2.39). The former is therefore the preferred representation of $f_{po}^{(o)}$ in this study.

3. One-term representation of $f_{po}^{(o)}$

For modeling purposes, we look for a one-term representation of $f_{po}^{(o)}$ and use an approximate sum rule to determine the associated parameter. A suitable candidate that satisfies both asymptotic behaviors would appear to be the first term in Eq. (2.39). Somewhat surprisingly, this representation does not give the best one-term fit to the molecular OOS we tested, even though it may be suited for simpler systems such as H, He, and H_2 . Instead, the one-term representation of $df_{po}^{(o)}/dE_p$ that gives the best overall performance is,

$$\frac{df_{po}^{(o)}}{dE_p} = \frac{b_o k_p}{(k_p^2 + \alpha_o^2)^3}, \quad (2.40)$$

with b_o a constant to be determined by an approximate sum rule. Note that the above expression forces the OOS to be zero at $k_p = 0$. Thus it does not necessarily match with the corresponding bound-bound transition at threshold. It also decreases too slowly at large k_p . However, the main goal of this study is integral cross sections. Modeling this quantity only requires the integral over $f_{po}^{(o)}$. It is not too surprising that the best one-term representation for the OOS of the five molecules studied here, Eq. (2.40), does not satisfy the limiting conditions. As a consequence, Eq. (2.40) is not a suitable expression to use in the study of the ejected-electron distribution. We believe that a more accurate representation of $f_{po}^{(o)}$, involving more than one term, is required in the study of the ejected-electron distribution. It should also be noted that many molecular OOSs, unlike H_2 , do not peak at $k_p = 0$. For example, the least square fit of experimental data

using Eq. (2.38) for several ionization channels in N_2 and CH_4 appear to indicate a threshold OOS value of zero.

We employ an approximate sum rule to estimate the value of b_o . Because of electron correlation, the Thomas-Reich-Kuhn (TRK) sum rule for a many-electron system cannot be decomposed into orbital contributions. However, if an approximate, effective one-electron Hamiltonian can be used to describe the active orbital φ_o , then the transition among its eigenstates will satisfy one-electron sum rules. One example of such effective Hamiltonian is the closed-shell Fock operator. Consider the integral in Eq. (2.33) with N_i representing the contribution of the photoionization process $o \rightarrow p$ to the sum rule. Assuming that the TRK sum rule for individual orbitals holds, and the bound-bound contribution to the sum rule is negligible, then $N_i \cong N_o$, with N_o the occupation number of φ_o . Equation (2.33) becomes

$$\int_0^\infty \frac{df_{po}^{(o)}}{dE_p} dE_p \cong N_o. \quad (2.41)$$

Analysis of the experimental OOS data for photoionization out of the valence orbitals of N_2 [27] and CH_4 [28] shows the above approximation works reasonably well for these cases. However, it works less well for the more tightly bound orbitals where double excitation may occur.

It is possible to determine b_o by substituting Eq. (2.40) into Eq. (2.41) and integrating over E_p . We find $b_o = 8\alpha_o^3 N_o / \pi$ and

$$\frac{df_{po}^{(o)}}{dE_p} = \frac{8\alpha_o^3 N_o k_p}{\pi(k_p^2 + \alpha_o^2)^3}. \quad (2.42)$$

It should be pointed out that Eq. (2.42) has a number of shortcomings. First, as pointed out earlier in this section, Eq. (2.42) does not take into account the correct asymptotic behavior of $f_{po}^{(o)}$ and thus is not expected to provide a reliable ejected-electron distribution. Second, it assumes that for excitation out of each orbital φ_o , there is only one ion state created, corresponding to the hole state φ_o^{-1} . Thus double excitations are not allowed. In the next section an example of CH_4 will be presented where experimentally it was shown that double excitation plays a role at moderate energies [28]. Third, it is assumed that all dipole-allowed excitations go to the ionization continuum. Obviously this assumption is never fully satisfied. However, because OOS is weighted by the excitation energy, the contribution from the ionization continuum dominates. The error introduced by neglecting the bound-bound transitions may be reasonably small. The present derivation suggests that subtracting the contributions from bound-bound transitions to Eq. (2.41) should improve the accuracy.

E. iBED model and a simplified version of this model (siBED)

The modified Mott cross section, with the incident-electron energy replaced by the average energy from the binary-encounter model, is given by

$$\frac{d\sigma_{po}^{BE}(E_p)}{dE_p} = \frac{8\pi N_o}{k_o^2 + \kappa_o^2 + \alpha_o^2} \left\{ \frac{1}{(k_p^2 + \alpha_o^2)^2} - \frac{1}{(k_p^2 + \alpha_o^2)(k_o^2 - k_p^2)} + \frac{1}{(k_o^2 - k_p^2)^2} \right\}. \quad (2.43)$$

Here κ_o^2 is twice the kinetic energy of the bound electron in φ_o . The above expression, called the binary-encounter cross section by Kim and Rudd, differs from the symmetric form of the binary-encounter cross section of Vriens [29] in the absence of the $1/(k_p^2 + \alpha_o^2)^3$ and $1/(k_o^2 - k_p^2)^3$ terms. Because the Mott cross section is a generalization of the Rutherford cross section for Coulomb scattering by taking exchange into account, the direct interaction term in Eq. (2.43) is obviously associated with the $\ell=0$ term in Eq. (2.29). On the other hand, the dipole-Born cross section is associated with the $\ell=1$ term in the two-electron Coulomb interaction and describes collisions of a different symmetry type than the modified binary-encounter cross section. Thus the two contributions should be additive. Neglecting the interference term between the two contributions, we obtain the singly differential-ionization cross section in the iBED model.

$$\begin{aligned} \frac{d\sigma_{po}^{iBED}(E_p)}{dE_p} &= \frac{8\pi N_o}{k_o^2 + \kappa_o^2 + \alpha_o^2} \left\{ \frac{1}{(k_p^2 + \alpha_o^2)^2} - \frac{1}{(k_p^2 + \alpha_o^2)(k_o^2 - k_p^2)} \right. \\ &\quad \left. + \frac{1}{(k_o^2 - k_p^2)^2} \right\} + \frac{8\pi}{k_o^2} \frac{df_{po}^{(o)}(E_p)}{dE_p} (k_p^2 + \alpha_o^2)^5 \\ &\quad \times \int_{K_{min}}^{K_{max}} \frac{1 + d_1 t + d_2 t^2}{K[(K + k_p)^2 + \alpha_o^2]^3 [(K - k_p)^2 + \alpha_o^2]^3} dK. \end{aligned} \quad (2.44)$$

In the BED model, Kim and Rudd [5] combined the dipole-Bethe and the binary-encounter cross sections with the constraint that the high-energy limit of the integrated-ionization cross section and the *total*-stopping cross section from the BED model agreed with their respective Bethe asymptotes. In the present case, it has been demonstrated in Sec. II C that the approximate dipole-Born cross section in Eq. (2.44) gives the Bethe asymptotes for both the integrated and stopping cross sections due to the ionization process $o \rightarrow p$. Furthermore, the high-energy limit of nondipole ionization decreases with T faster than the dipole term and does not contribute to the Bethe asymptote. Since the Bethe asymptotes are already built in, they can no longer be used as a guide for combining the Born and binary-encounter contributions.

While the integrated cross section from the binary-encounter term in Eq. (2.44) decreases faster than $\ln(T)/T$ and does not contribute to the Bethe asymptote for this quantity, it does contribute to the Bethe asymptote for the stopping cross section. This is a shortcoming of the binary-encounter model. By requiring the sum of the binary-

encounter and dipole-Born contributions to the stopping cross section equal to the *total*-stopping cross section, as done in the BED model, would incorporate extraneous constraints outside the ionization process. Thus for the iBED model we choose to add the two contributions together without any additional constraint.

The integrated cross section σ_{po} is obtained by integrating Eq. (2.44) over E_p . For the binary-encounter term that has a symmetrized expression including both direct and exchange contributions, the integration limit is from 0 to $(T - \mathcal{E}_o)/2$. For the dipole-Born term, the integration limit is from 0 to $T - \mathcal{E}_o$ because it includes direct collisions only.

$$\begin{aligned} \sigma_{po}^{iBED} = & \frac{4\pi N_o}{k_o^2 + \kappa_o^2 + \alpha_o^2} \left[\frac{k_o^2 - \alpha_o^2}{k_o^2 \alpha_o^2} - \frac{1}{(k_o^2 + \alpha_o^2)} \ln \left(\frac{k_o^2}{\alpha_o^2} \right) \right] \\ & + \frac{8\pi}{k_o^2} \int_0^{(k_o^2 - \alpha_o^2)/2} (k_p^2 + \alpha_o^2)^5 \frac{df_{po}^{(o)}(E_p)}{dE_p} dE_p \\ & \times \int_{K_{min}}^{K_{max}} \frac{1 + d_1 t + d_2 t^2}{K[(K + k_p)^2 + \alpha_o^2]^3 [(K - k_p)^2 + \alpha_o^2]^3} dK. \end{aligned} \quad (2.45)$$

In the absence of experimental or theoretical data for $f_{po}^{(o)}$, the approximate one-term expression in Eq. (2.42) can be used and we obtain the simplified version of the improved binary-encounter dipole (siBED) model,

$$\begin{aligned} \sigma_{po}^{siBED} = & \frac{4\pi N_o}{k_o^2 + \kappa_o^2 + \alpha_o^2} \left[\frac{k_o^2 - \alpha_o^2}{k_o^2 \alpha_o^2} - \frac{1}{(k_o^2 + \alpha_o^2)} \ln \left(\frac{k_o^2}{\alpha_o^2} \right) \right] \\ & + \frac{64\alpha_o^3 N_o}{k_o^2} \int_0^{(k_o^2 - \alpha_o^2)/2} k_p (k_p^2 + \alpha_o^2)^2 dE_p \\ & \times \int_{K_{min}}^{K_{max}} \frac{1 + d_1 t + d_2 t^2}{K[(K + k_p)^2 + \alpha_o^2]^3 [(K - k_p)^2 + \alpha_o^2]^3} dK. \end{aligned} \quad (2.46)$$

As discussed earlier, the binary-encounter contribution in the iBED and siBED cross sections are of symmetry type $\ell=0$. Due to the difference in symmetry, the short-range interactions described by the binary-encounter contribution do not cause redundancy problems with the shielding part of the shielded-dipole interaction described by the dipole Born contribution.

III. NUMERICAL EXAMPLES

Total ionization cross sections for N_2 , H_2O , CO_2 , CH_4 , and CF_4 have been calculated to illustrate the applicability of the iBED and siBED models. These five molecules are chosen because recent experimental data from the Rice group for these molecules [30–35] have tight error bounds, $\pm 5\%$, and hence well suited as a benchmark for our models. For N_2 , H_2O , CO_2 , and CH_4 , a recent recalibration of the apparatus by the Rice group results in data that differ slightly from those in the original publications [35]. The revised data are used as benchmark. For these four molecules, an older set of

experiment by Rapp and Englander-Golden [36] has the next-tightest error estimate of $\pm 7\%$. Both CH_4 and CF_4 have Jahn-Teller splitting. Comparing the results of these two molecules may be of interest. Also, CF_4 is used as a feed gas for plasma etching. A large pool of experimental data on this molecule has been reviewed [37,38]. Among the reviewed data the measurement of Nishimura *et al.* [9] has the smallest error estimate, $\pm 7.5\%$, and it will also be included as a benchmark for our calculations. For all five molecules considered, a wealth of experimental data are available besides what we use for benchmarking. However, for clarity in the presentation of the figures, we choose to compare only with a more selected set.

As in the case of BED/BEB model, most of the computational effort is spent on quantum-chemistry calculations to determine the molecular parameters: the binding energy ($= -\alpha_o^2/2$) and kinetic energy of the bound electron ($= \kappa_o^2/2$). In the iBED/siBED model, the latter is used only in the binary-encounter part of the calculation. All quantum-chemistry calculations were done using the experimental-equilibrium geometry of the neutral molecule. The effect of nuclear motion has been neglected except in CH_4 and CF_4 . For CH_4 the large Jahn-Teller splitting observed in the ion is accounted for in the iBED calculation. For CF_4 a rough estimate of the Jahn-Teller effect is given. The quantum-chemistry calculations use the augmented correlation-consistent aug-cc-pVQZ basis of Gaussian functions [39] for N_2 , H_2O , CO_2 , and CH_4 . For CF_4 the augmented correlation-consistent aug-cc-pVTZ basis [39] is used. The kinetic energies, being a one-electron property, are determined using Hartree-Fock calculations. The binding energies are either taken from experimental vertical ionization potentials (VIP) or from *ab initio* calculations. In the *ab initio* calculations the VIP to the lowest-ion state of each symmetry is determined by taking the difference between the total energies for the target and the ion states using the RCCSD(T) (spin-restricted coupled-cluster singles and doubles with perturbation correction for triples) method [40,41]. Since size-consistency is not a problem for RCCSD(T), it is well suited for determining the energy difference between two systems with different number of electrons. However, RCCSD(T) can only be used to determine the lowest IP of each symmetry. The energies of the second and higher ion states of a symmetry and the corresponding IPs are determined using CASSCF calculations and the result scaled by the RCCSD(T) result for the lowest state. For N_2 , internally contracted multireference configuration interaction calculations [42] are used to search for the $(2\sigma_g^{-1})$ hole state. All theoretical calculations have been carried out using MOLPRO [43]. The agreement between theory and tabulated experimental data [44] are consistently good, giving confidence that the set of molecular parameters used in our calculations are the best available set.

The two-dimensional integration over K and E_p are carried out numerically using Simpson's rule. The calculated partial cross sections σ_{po}^{iBED} are added up to give the total ionization cross section,

$$\sum_p \sum_o \sigma_{po}^{iBED} = \sigma^{iBED}. \quad (3.1)$$

The siBED model assumes only one ion state is produced from the ionization of φ_o , so the label p is dropped,

$$\sum_o \sigma_o^{siBED} = \sigma^{siBED}. \quad (3.2)$$

The results using the iBED and siBED models are described separately below. In the iBED calculations, we use the OOS from available experimental data. The optimal values for the coefficients d_1 and d_2 in the expression for the dipole-Born cross section are determined by the best fit to experimental total ionization cross section. The goal is to investigate the nature of the shielding of the dipole potential. In the siBED calculations, our goal is to derive a set of parameters that is applicable to all five molecules under study. The calculated cross sections are compared with the BEB cross sections as well as experiment. Note that other theoretical models for electron-impact ionization cross sections are also available. One frequently used model is the semiclassical Deutsch-Märk model [45]. Nevertheless, we have limited our comparison to the BEB model in order to illustrate the difference between the use of Bethe and dipole-Born cross sections.

A. Calculations using the iBED model

1. N_2

The OOS for the photoionization of N_2 has been measured by Hamnett *et al.* [27] from threshold to 50 eV in an ($e,2e$) coincidence experiment. They reported $f_{po}^{(o)}$ for the production of the ion states $X^2\Sigma_g^+$ ($3\sigma_g$ hole), $A^2\Pi_u$ ($1\pi_u$ hole), $B^2\Sigma_u^+$ ($2\sigma_u$ hole), and $2^2\Sigma_g^+$ ($2\sigma_g$ hole). They also reported the production of an ion state that they named Z state because it does not relate to a specific hole state. The VIP for the $2\sigma_g$ hole listed in Levin and Lias [44] varies from 28–29 eV to 38.9 eV. We investigated the nature of the Z state and the $2\sigma_g$ hole state by carrying out state-averaged (10 electron/12 orbital) CASSCF calculations followed by ICMRCI for the lowest six N_2^+ states of $2^2\Sigma_g^+$ symmetry. We could not locate a pure $2\sigma_g$ hole state. The second $2^2\Sigma_g^+$ state was the first state with significant $2\sigma_g$ hole character. Its VIP was 29.20 eV, in good agreement with the ≈ 29 eV threshold that Hamnett *et al.* reported for their Z state and the lowest estimated VIP of 28–29 eV by Levin and Lias. The configuration $1\sigma_g^2 1\sigma_u^2 2\sigma_g^2 2\sigma_u^2 1\pi_{ux}^2 1\pi_{uy}^2 3\sigma_g^2$ had a weight coefficient of -0.3433 , but two configurations corresponding to double excitations, $1\sigma_g^2 1\sigma_u^2 2\sigma_g^2 2\sigma_u^2 1\pi_{ux}^2 1\pi_{uy}^2 3\sigma_g^2 1\pi_{gx}^2$ and $1\sigma_g^2 1\sigma_u^2 2\sigma_g^2 2\sigma_u^2 1\pi_{ux}^2 1\pi_{uy}^2 3\sigma_g^2 1\pi_{gy}^2$, had weight coefficients of 0.5333. Thus the Z state was not a pure hole state, but had characteristics of both a doubly excited state and a hole state. The third to sixth $2^2\Sigma_g^+$ states, corresponding to VIPs 33.43–37.99 eV, all exhibited the character of a mixed $2\sigma_g$ hole state and doubly excited states. None could be characterized as a pure $2\sigma_g$ hole state.

In our iBED calculation, we fitted the experimental $f_{po}^{(o)}$ using three-, four-, and five-term expansions of Eq. (2.38) for the $X^2\Sigma_g^+$, $A^2\Pi_u$, and $B^2\Sigma_u^+$ data, and three-term expansions for the Z state and what Hamnett *et al.* [27] labeled as $2\sigma_g$ hole state. The optimal length of expansion was determined by the shortest expansion that satisfied the following three criteria: (1) The OOS should be positive at all electron energies. (2) The f sum obtained should be physically reasonable. (3) The fit should have a reasonable root-mean-square error after satisfying conditions (1) and (2). For the $B^2\Sigma_u^+$ and Z states, we found the first coefficient in the fit, corresponding to the value of $f_{po}^{(o)}$ at zero ejected-electron energy, to be consistently negative for any reasonable value of f sum. Thus the final fit for these two cases was obtained by forcing the first coefficient to be zero. The oscillator-strength sums from the fit were 2.251 for the photoionization of an electron out of the $3\sigma_g$ orbital, 3.464 for $1\pi_{ux} + 1\pi_{uy}$, 0.739 for the $2\sigma_u$, 0.301 for the Z hole, and 1.085 for $2\sigma_g$. For $2\sigma_u$ and $2\sigma_g$ hole states, the f sum was far from the orbital occupation number of 2, even after including the contribution of the Z state. We believe this to be partially due to the limited-energy range in the experimental data so that for the more tightly bound orbitals there are larger uncertainties in the extrapolation.

Due to the uncertainty in the nature of the Z state and the $2\sigma_g$ hole state, two iBED calculations have been carried out for N_2 . The first iBED calculation, labeled as iBED(1), treated the Z state as the lowest $2\sigma_g$ hole state and the ion state observed by Hamnett *et al.* [27] at 37.8 eV as an excited state associated with the $2\sigma_g$ hole. This treatment was consistent with the quantum-chemistry result for N_2^+ states of $2^2\Sigma_g^+$ symmetry. The VIP used, together with their sources, were: $3\sigma_g$, 15.58 (expt., Ref. [44]), $1\pi_u$, 16.98 [RCCSD(T)], $2\sigma_u$, 18.78 [RCCSD(T)], and $2\sigma_g$ forming excited ion, 37.8 eV (expt., Ref. [27]). A VIP of 29.20 eV for the production of the Z state of the ion, based on a scaled CAS calculation, was used. Note that our RCCSD(T) calculation for the VIP of $3\sigma_g$ was 15.60 eV, in good agreement with experiment. RCCSD(T) VIPs for other ion states were expected to be of similar level of accuracy. Because the binary-encounter model was based on the collision between a free and a bound electron, it could not describe ionization resulting in an excited-ion state, such as the higher $2\sigma_g$ hole state. Hence excited-ion states were not included in the calculation of binary-encounter cross section. The occupation numbers from the SCF configuration of the neutral molecule were used for N_o in all the binary-encounter calculations. Thus for the $2\sigma_g$ hole, we used $N_o=2$ for the Z state and the binary-encounter contribution from the 37.8 eV $2\sigma_g$ hole state was neglected.

Due to the lack of experimental OOS, the contributions from the core orbitals, $1\sigma_g$ and $1\sigma_u$, were calculated using the siBED model. However, the contributions from these two orbitals were very small. At 1 keV electron energy their contribution was only $0.003 \times 10^{-20} \text{ m}^2$. Thus their contributions could be safely neglected.

Based on the molecular parameters described above, iBED calculations were carried out to determine the param-

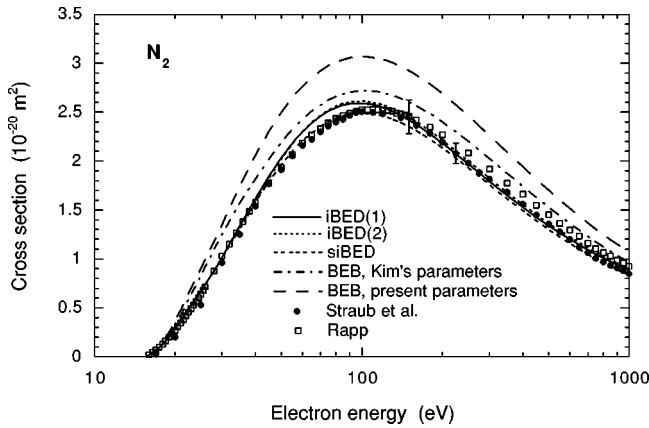


FIG. 1. Total-ionization cross section of N_2 calculated using the iBED and siBED models. Two sets of iBED calculations, iBED(1) and iBED(2), corresponding to different treatments of the doubly excited state, are shown. Also presented are the experimental data of Straub *et al.* [30] and Rapp and Englander-Golden [36]. The BEB cross sections using Kim's molecular parameters and the parameters determined in this study are included for comparison.

eters d_1 and d_2 in the Born cross section by a fit to the experimental data of Straub *et al.* [30] and Rapp and Englander-Golden [36]. Since the contributions from the d_1 term became important near the peak of the cross-section curve and the d_2 term was relatively unimportant until the energies were higher, we determined d_1 first by fitting the cross-section peak. Then d_2 was determined using the high-energy data. The values $d_1 = -2.0$ and $d_2 = 0.5$ have been chosen in this manner.

The second iBED calculation, iBED(2) used the same set of VIPs as (1), but treated the Z state as a doubly excited state associated with the $2\sigma_u$ hole. The binary-encounter contribution was calculated using $N_o = 2$ for the $B^2\Sigma_u^+$ state and the 37.8 eV $2\sigma_g$ hole state. The contribution of the Z state was neglected. The ionization cross sections calculated using both iBED models are presented in Fig. 1. As seen from Fig. 1, the iBED(1) and iBED(2) cross sections are very close. Thus electron-impact ionization data cannot be used to determine if the Z state should be labeled as a $2\sigma_g$ hole state or a doubly excited state associated with the $2\sigma_u$ hole. Figure 1 will be further discussed in Sec. III B 1 when the siBED cross sections for N_2 are presented.

2. CH_4

In an electron-ion coincidence experiment, Backx and Van der Wiel [28] measured the OOS for the production of $(1t_2^{-1})$, $(2a_1^{-1})$, and a third, two-electron excited state that they labeled as "higher states." In addition, Backx *et al.* [46] reported coincidence experiment of the high-energy, scattered electron and the essentially zero-energy ejected electron. Their spectra clearly showed the Jahn-Teller splitting of the ion state labeled as $(1t_2^{-1})$. The equilibrium geometry of the ion corresponding to the $1t_2$ hole has a lower symmetry, C_{3v} , than the T_d symmetry of the neutral molecule. The triple degeneracy of the 2T_2 state is lifted and the ion splits into two states, 2A_1 and 2E , the latter being doubly degen-

erate. The threshold electron spectrum for 2A_1 peaks at ≈ 13.5 eV, and 2E spectrum peaks at ≈ 14.5 eV. In their analysis, Backx and van der Wiel used 13.5 eV as the threshold of the $(1t_2^{-1})$ OOS and lumped the contributions from the 2A_1 and 2E states together. They also identified the two-electron excited state with the configuration $1t_2^4 2a_1^2 3a_1^1$.

In order to understand how the Jahn-Teller effect influences the photoionization cross section, we fitted the OOS for the $(1t_2^{-1})$ state in three different ways. (1) Following Backx and van der Wiel, we used 13.5 eV as the VIP and lumped the 2A_1 and 2E states together. A five-term expansion for the OOS gave an ionization f sum of 5.93 and the average % difference between the fit and experiment was 6.0%. (2) A VIP of 13.5 eV was used for the 2A_1 state and 14.5 eV for the 2E state. The OOS of the two states were constrained to use the same set of expansion coefficients, except that different VIPs are used for α_o^2 [see Eq. (2.38)]. A range of expansion lengths, from two to seven terms, was tried. In all cases, the fitting of the low-energy OOS worked well but the OOS at the high-energy end consistently had large fitting errors, as much as $\pm 50\%$. (3) Two VIPs, 13.5 and 14.5 eV, were used for the two Jahn-Teller states and the expansion coefficient were allowed to vary freely. We obtained the poorest fit in this case. The f sums for the two sets of OOS were unphysical. The above three fittings seem to indicate that the OOS is best approximated by a single VIP, as practiced in the data analysis of Backx and Van der Wiel [28], but it is difficult to reconcile this result with the Jahn-Teller effect indicated by the zero-energy e - $2e$ coincidence experiment.

The OOS for the $(2a_1^{-1})$ state was fitted using a five-term expansion and a VIP of 22 eV. The f sum from the fit was 0.57. A five-term expansion with 29 eV for the VIP is used for the two-electron excited state, giving 0.44 for the f sum. Both VIPs were values suggested by Backx and Van der Wiel [28]. In both fittings, the first coefficient in the expansion, corresponding to the value of $f_{po}^{(o)}$ at zero energy, was set to zero. Otherwise we either obtained unphysical f values at some electron energy or unphysical f sums. Also, as in the case of ionization of the inner orbitals of N_2 , the f sum for the ionization of the $2a_1$ orbital of CH_4 did not match its occupation number, even though the f sum for the $(1t_2^{-1})$ hole was close to its occupation number of 6.

Two iBED calculations were carried out to test the role of Jahn-Teller effect in CH_4 . In iBED(1), the Jahn-Teller effect was accounted for by assigning 13.5 and 14.5 eV for the VIP of the 2A_1 and 2E state, respectively, with 1/3 of the OOS assigned to 2A_1 and 2/3 to 2E . The $(2a_1^{-1})$ state and the doubly excited state were explicitly accounted for in the Born calculation, but the binary-encounter calculation excluded the doubly excited state and $N_o = 2$ was used for the $(2a_1^{-1})$ state. The coefficients d_1 and d_2 in the Born cross section are chosen based on a fit to the experimental data of Straub *et al.* [33] and Rapp and Englander-Golden [36]. The optimal choice was $d_1 = -0.4$, $d_2 = 0.2$.

In iBED(2), Jahn-Teller splitting in $(1t_2^{-1})$ was neglected and a VIP of 13.5 eV was used for all electrons in the $1t_2$

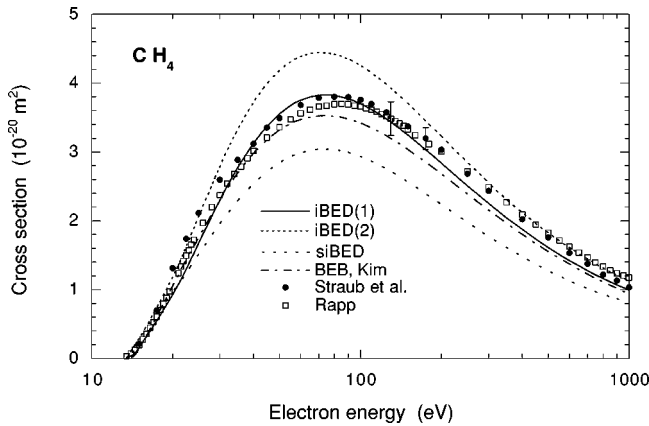


FIG. 2. Total ionization cross section of CH_4 calculated using the iBED and siBED models. Two sets of iBED calculations, iBED(1), which includes Jahn-Teller splitting, and iBED(2), which neglects Jahn-Teller splitting, are shown. Also presented are the experimental data of Straub *et al.* [33] and Rapp and Englander-Golden [36], plus the BEB cross sections of Kim *et al.* [7].

orbital. The treatment of the $(2a_1^{-1})$ state and the doubly excited state were identical with iBED(1). Figure 2 presents the two iBED cross sections as well as the experimental cross section of Straub *et al.* [33] and Rapp and Englander-Golden [36]. Of the two theoretical cross sections, the iBED(1) data are close to experimental values of Straub *et al.* at 35 eV and above. Below 35 eV they become closer to the data of Rapp and Englander-Golden. The iBED(2) cross sections are larger than both sets of experimental data except below 30 eV and above 200 eV. Below 30 eV it becomes quite close to the data of Straub *et al.* Overall, it appears that accounting for the Jahn-Teller effect in the t_2^{-1} state is important to obtain a good fit to experiment. There appears to be a slight hump in the data of Straub *et al.* around the 20–30 eV region, but it is absent in the data of Rapp and Englander-Golden. It should be pointed out that Straub *et al.* reported higher light ion productions than previous experiments [47–50]. This is attributed to a better collection technique used by the Rice group and provides a possible explanation for the difference between the two sets of experimental data. We shall return to Fig. 2 when we discuss the siBED cross sections for CH_4 in Sec. III B 4.

It is worthwhile to compare the two sets of parameters, d_1 and d_2 for N_2 and CH_4 , both obtained by a fit to the experimental cross-section data. In the N_2 case the parameter d_1 is large and negative, -2.0 . Since it is opposite in sign to the leading dipole term, it represents a repulsive short-range potential acting as the shielding potential. The parameter d_2 is smaller and positive, 0.5 , representing a small attractive correction to the repulsive shielding term represented by d_1 . For CH_4 , the parameters are $d_1 = -0.4$ and $d_2 = 0.2$, indicating a shielding potential that is slightly repulsive. The two sets of d_1, d_2 values appear to be related to the nature of the chemical bond in the two molecules. Because N_2 has a triple bond, electron-charge distribution builds up at the center of the molecule. It is reasonable for the incoming electron to experience a strong repulsive potential as it comes near. CH_4 , on the other hand, has four single bonds extending in a tetrahe-

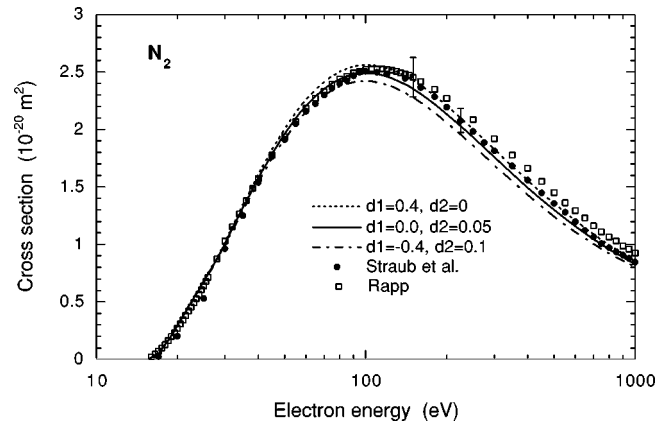


FIG. 3. Total ionization cross section of N_2 calculated using the siBED model as a function of the parameter d_1 . The experimental data of Straub *et al.* [30] and Rapp and Englander-Golden [36] are also presented for comparison.

dron. It has a more open structure and the short-range interaction probably is only slightly repulsive.

B. Calculations using the siBED model

The preceding discussion shows d_1 and d_2 to be molecular specific parameters and related to the nature of the molecular charge distribution in the bonding region. In this section, we approach the problem in a different manner. As in the case of the one-term representation of $df_{po}^{(o)}/dE_p$, we look for a set of generic d_1 and d_2 applicable to siBED calculations for all five molecules. This is done by choosing a set of values that gives the optimal representation in the siBED calculations of N_2 , H_2O , and CO_2 . Figure 3 shows how σ^{siBED} of N_2 varies with d_1 and d_2 . As discussed in Sec. II B, d_1 and d_2 have no effect at the low-energy cross section but improve the agreement of the overall cross section with the experiment of Straub *et al.* [30] and Rapp and Englander-Golden [36]. With d_1 changing in step of 0.4 , the change of the cross section is small and smooth. Also, once d_1 is chosen, the parameter d_2 is determined by an optimal representation of the high-energy part of the cross-section curve. The effect on the H_2O and CO_2 results is similar. Based on these calculations, the values $d_1 = 0.0$ and $d_2 = 0.05$ are chosen and these values will be used for all five molecules.

I. N_2

The siBED cross sections of N_2 were calculated using the same set of molecular parameters as the iBED(1) calculation. The Z state was used to represent the $2\sigma_g$ hole and the contributions from the 37.8 eV state was neglected. Figure 1 presents the siBED cross sections together with the two iBED cross sections and the experimental data of Straub *et al.* [30] and Rapp and Englander-Golden [36]. The iBED(1), iBED(2), and siBED cross sections are in good agreement with one another and the experimental data except near the cross-section peak. There the iBED calculations overestimate the cross section slightly. Note that the values

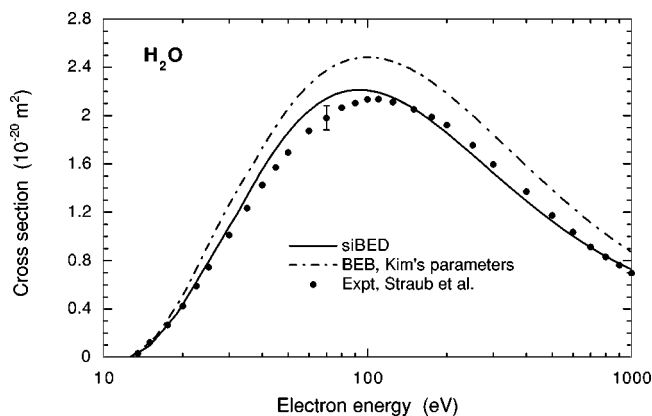


FIG. 4. Total ionization cross section of H_2O calculated using the siBED model. Also presented are the experimental data of Straub *et al.* [31] and the BEB cross sections of Hwang *et al.* [6].

of d_1 and d_2 used for the iBED and siBED calculations are very different, representing a different description of the short-range part of the shielded-dipole potential. It appears that the inaccuracies in the one-term approximation of the OOS used in the siBED calculation is partially compensated by a more weakly shielded dipole potential, resulting in total ionization cross sections that are in overall agreement with experiment and with the iBED results. However, as pointed out in Sec. II D 3 the siBED model does not provide a reliable secondary-electron energy distribution whereas the iBED results, based on experimental OOS, should be able to do so.

Also presented in Fig. 1 are two BEB cross sections, σ^{BEB} , calculated using the parameters determined by Hwang *et al.* [6] and using the same set of parameters employed in the $\sigma^{iBED(1)}$ and σ^{siBED} calculations. Both BEB cross sections are larger than iBED(1), iBED(2), siBED, and experimental data. Notice that the set of VIPs used by Hwang *et al.*, except for the $3\sigma_g$ hole, are determined using Hartree-Fock calculations. Their values are consistently higher than the VIPs determined here. Hence the σ^{BEB} calculated using the present set of parameters are larger than the σ^{BEB} reported by Hwang *et al.* This is also the case for all molecules studied.

2. H_2O

Figure 4 presents the siBED calculations of H_2O , together with the experimental data of Straub *et al.* [31] and the BEB cross sections of Hwang *et al.* [6]. The VIPs used in the siBED calculations are 12.61 for $1b_1$ [expt, Ref. [44]], 14.75 for $3a_1$ [expt, Ref. [44]], 18.74 for $1b_2$ [expt, Ref. [44]], and 32.61 eV for $2a_1$ [expt, Ref. [44]]. As in the case of N_2 , we find the siBED cross sections are in better agreement with experiment than the BEB result. Note also that a BEB calculation using the present set of VIP will give even larger cross sections. Both the siBED and BEB cross sections are larger than the experimental cross sections around the low-energy side of the cross-section peak. This is the energy range where the largest deviation between the siBED model and experiment is found.

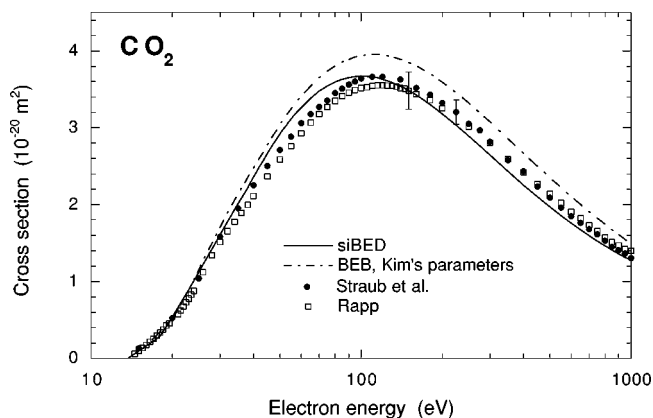


FIG. 5. Total ionization cross section of CO_2 calculated using the siBED model. Also presented are the experimental data of Straub *et al.* [32] and Rapp and Englander-Golden [36], plus the BEB cross sections of Hwang *et al.* [6].

3. CO_2

The siBED cross sections for CO_2 are presented in Fig. 5, together with the experimental data of Straub *et al.* [32] and Rapp and Englander-Golden [36], plus the BEB cross sections of Hwang *et al.* [6]. The VIPs used in the siBED calculations are 13.73 for $1\pi_g$ [expt, Ref. [44]], 17.85 for $1\pi_u$ [RCCSD(T)], 18.16 for $3\sigma_u$ [RCCSD(T)], 19.45 for $4\sigma_g$ [RCCSD(T)], 37.79 for $2\sigma_u$ (CASSCF), and 39.16 eV for $3\sigma_g$ (CASSCF). The RCCSD(T) value for the first VIP is 13.88 eV. As in the case of H_2O , the siBED cross sections are in better agreement with experimental data than the BEB cross sections, especially at higher energies. Also, the overall agreement is better with the data of Straub *et al.* than with Rapp and Englander-Golden. Except for the $1\pi_u$ orbital, the BEB cross sections were calculated using the Hartree-Fock VIPs. Thus the BEB cross sections will be significantly higher if the present set of VIPs are used.

4. CH_4

The siBED calculations for CH_4 neglected the Jahn-Teller splitting in the $(1t_2^{-1})$ channel and used 13.5 eV as the VIP for the $1t_2$ orbital. It also neglected the contribution from the doubly excited state with a VIP at 29 eV. Both Born-dipole and binary-encounter calculations used $N_o=2$ for the $(2a_1^{-1})$ channel.

The siBED cross sections are presented in Fig. 2, together with the iBED cross sections, the experimental cross sections of Straub *et al.* [33] and Rapp and Englander-Golden [36], and the BEB cross section of Kim *et al.* [7]. Unlike the N_2 case where the siBED and iBED cross sections employing the same set of molecular parameters are in good agreement with each other, we find significant differences between the siBED and iBED cross sections, both with each other and with experiment. The siBED and iBED(1) cross sections differ by 21% at the cross-section peak. While the two sets of calculations use slightly different values of d_1 and d_2 , it appears that the major source of the difference comes from the OOS. The use of experimental OOS greatly improves the agreement with measured data. This is one case where the

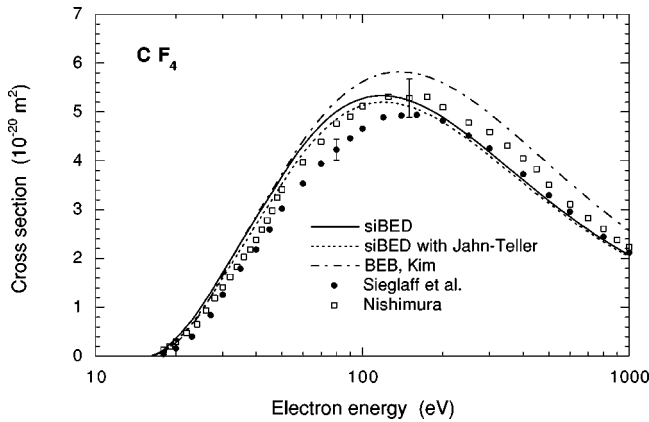


FIG. 6. Total ionization cross section of CF_4 calculated using the siBED model. Also presented are the experimental data of Sieglaff *et al.* [34] and Nishimura *et al.* [9], plus the BEB cross sections of Nishimura *et al.* [9].

one-term approximation for the OOS is insufficient and a reasonable representation of the total ionization cross section requires experimental OOS data.

The BEB cross section of Kim *et al.* is between the iBED and siBED results. The agreement with Rapp and Englander-Golden's data [36] is very good from threshold to the cross-section peak. The agreement with the recent data of Straub *et al.* is not as good. In view of the fact the OOS fitted from experimental data is quite different from the OOS used by Kim *et al.* [7], the agreement found between the BEB result and experiment is probably due to the use of the energy-scaled Bethe cross section in the BEB calculation, which tends to overestimate the cross section and, in this case, partially compensates for the shortcoming in the OOS.

5. CF_4

Calculations of siBED cross sections have been carried out using the following values for the VIP: 16.30 eV for $1t_1$ [expt, Ref. [44]], 17.49 for $4t_2$ [RCCSD(T)], 18.41 for $1e$ [RCCSD(T)], 22.64 for $3t_2$ (CASSCF), and 25.86 eV for $4a_1$ (CASSCF). All other parameters were deduced from Hartree-Fock calculations and have been tabulated previously [9]. Figure 6 presents the siBED and BEB [9] cross sections as well as the experimental data of Sieglaff *et al.* [34] and Nishimura *et al.* [9]. The two sets of theoretical cross sections are in excellent agreement with each other at low energies and both are larger than the experimental data. Above 80 eV, the two sets of theoretical data differ, with the siBED cross section coming to close agreement with experiment.

Like CH_4 , Jahn-Teller effect should play a role in the ionization of CF_4 . To understand the role of Jahn-Teller effect, we have carried out the calculation with two ion states in C_{3v} symmetry. The $1t_1$ orbital in T_d symmetry was split into two components, the nondegenerate a_2 component and the doubly degenerate e component. As a rough approximate, we used the Jahn-Teller splitting observed in CH_4 and raised the VIP of the a_2 orbital by 1 eV. The $4t_2$ orbital was split into an a_1 component and e component in C_{3v} symmetry.

Again we used 1 eV as the Jahn-Teller splitting for this orbital. The siBED cross sections calculated in this manner are labeled as siBED with Jahn-Teller in Fig. 6. This simple introduction of Jahn-Teller effect improves the siBED result with experiment, particularly with the data of Nishimura *et al.*, but insufficient to account the difference between siBED results and the data of Sieglaff *et al.*

Note that the BEB calculations in Fig. 6 were done using Hartree-Fock data, as is the case of the other molecules in this study. Indeed, Nishimura *et al.* pointed out that BEB cross sections for CF_4 calculated using Hartree-Fock parameters gave results in better agreement with experiment than CASSCF parameters. They chose the BEB cross sections determined using the Hartree-Fock parameters as the "recommended" cross section. Here we show that in the siBED model, parameters determined from correlated calculations are important to bring theory into closer agreement with experiment. The earlier conclusion that Hartree-Fock parameters should be "best suited" is a fortuitous result due to the use of energy-scaled Bethe cross sections.

IV. SUMMARY

The approximate GOS and OOS derived here, based on variables deduced from the singularities of these quantities on the complex K plane or k_p plane and incorporating known limiting behavior, enable us to use the dipole-Born cross section instead of an energy-scaled Bethe cross section in the binary-encounter-dipole model. Furthermore, the dipole-Born cross section includes the effect due to the shielding of the long-range dipole potential. The iBED model so derived provides a viable method to analyze electron-impact ionization cross sections and are capable of incorporating finer details of molecular interactions such as doubly excited states and Jahn-Teller splitting. These issues in electron-impact ionization cross sections have not been treated by calculations previously.

The siBED model is developed to provide a means to calculate approximate total ionization cross sections based on known molecular parameters. Here a simple one-term approximation of the OOS is used instead of the experimental OOS. The parameters d_1 and d_2 are chosen to represent the shielding of a generic dipole potential, instead of a molecular specific potential. For N_2 , H_2O , CO_2 , and CF_4 , the siBED model works quite well, but in the case of CH_4 , it underestimates the ionization cross section by $\approx 21\%$ at the peak, demonstrating the importance of reliable OOS data.

The role of Jahn-Teller effects in electron-impact ionization are investigated for CH_4 and CF_4 . For CH_4 , the fit of OOS works best if a single VIP is used for the Jahn-Teller state, 2T_2 . However, the iBED cross sections agree much better with the experiment of Straub *et al.* [33] if Jahn-Teller splitting is incorporated. For CF_4 , we simulate the Jahn-Teller effect by introducing splittings in both the $1t_1$ and $4t_2$ hole states. The resulting cross section is in better agreement with experimental data than the calculation without the Jahn-Teller effect, but below 200 eV there is still a sizeable difference between the siBED data and the data of Sieglaff *et al.* [34]. It is uncertain at present whether this is due to the

approximate OOS used or inaccurate description of the Jahn-Teller effect. Future experiment measurements or quantum-chemistry studies of the Jahn-Teller splitting of CF_4^+ ion will be very useful to determine the role of the Jahn-Teller effect on the ionization of CF_4 .

In this study, the parameters d_1 and d_2 used in the shielding of the long-range dipole potential have been chosen by fitting experimental data. Analysis of the calculations indicate that they are related to the molecular charge distribution. Further studies are required to relate these two parameters with molecular properties in a quantitative manner.

As in the case of the Lassetre series for the GOS of bound-bound excitations, the series expansion for the GOS derived here should be useful in the analysis and extension of experimental data of electron-impact ionization.

ACKNOWLEDGMENTS

A critical reading of this paper by Dr. Y.-K. Kim is appreciated. I also thank Dr. Bernard Lindsay for sending his revised cross-section data. This work was supported by the NASA Ames IPT on devices and nanotechnology.

-
- [1] I. Bray and A. Stelbovics, Phys. Rev. Lett. **69**, 53 (1992); **70**, 746 (1993).
- [2] K. Bartschat, E. Hudson, P. Scott, P. Burke, and V. Burke, J. Phys. B **29**, 115 (1996); Phys. Rev. A **54**, R998 (1996).
- [3] T.N. Rescigno, M. Baertschy, W.A. Issacs, and C.W. McCurdy, Science **286**, 2474 (1999).
- [4] F. Robicheaux, M.S. Pindzola, and D.R. Plante, Phys. Rev. A **55**, 3573 (1997).
- [5] Y.-K. Kim and M.E. Rudd, Phys. Rev. A **50**, 3954 (1994).
- [6] W. Hwang, Y.-K. Kim, and M.E. Rudd, J. Chem. Phys. **104**, 2956 (1996).
- [7] Y.-K. Kim, W. Hwang, N.M. Weinberger, M.A. Ali, and M.E. Rudd, J. Chem. Phys. **106**, 1026 (1997).
- [8] M.A. Ali, Y.-K. Kim, W. Hwang, N.M. Weinberger, and M.E. Rudd, J. Chem. Phys. **106**, 9602 (1997).
- [9] H. Nishimura, W.M. Huo, M.A. Ali, and Y.-K. Kim, J. Chem. Phys. **110**, 3811 (1999).
- [10] W.M. Huo and Y.K. Kim, Chem. Phys. Lett. **319**, 576 (2000).
- [11] S.P. Khare, M.K. Sharma, and S. Tomar, J. Phys. B **32**, 3147 (1999).
- [12] S.P. Khare, S. Tomar, and M.K. Sharma, J. Phys. B **33**, L59 (2000).
- [13] W.M. Huo, J. Chem. Phys. **56**, 3468 (1972).
- [14] W.M. Huo, J. Chem. Phys. **57**, 4800 (1972).
- [15] M. Inokuti, Rev. Mod. Phys. **43**, 297 (1971).
- [16] E.N. Lassetre, A. Skerbele, and M.A. Dillon, J. Chem. Phys. **50**, 1829 (1969).
- [17] H. Bethe, Ann. Phys. (Paris) **5**, 325 (1930).
- [18] E.N. Lassetre, J. Chem. Phys. **43**, 4479 (1965).
- [19] W.M. Huo, J. Chem. Phys. **71**, 1593 (1979).
- [20] Z. Felfli, A.Z. Msezane, and D. Bessis, Phys. Rev. Lett. **81**, 963 (1998).
- [21] A.R.P. Rau and U. Fano, Phys. Rev. **162**, 68 (1967).
- [22] One-electron orthogonality between two wave functions means the integral of their one-electron transition density is zero. See I. Shavitt, *Methods of Electronic Structure Theory*, The Method of Configuration Interaction, edited by H. F. Schaefer III (Plenum Press, New York, 1977), p. 239.
- [23] H.S.M. Massey and C.B.O. Mohr, Proc. R. Soc. London, Ser. A **132**, 605 (1931).
- [24] M.C. Walske, Phys. Rev. **88**, 1283 (1952).
- [25] A.R. Holt, J. Phys. B **2**, 1209 (1969).
- [26] M. Inokuti, M.A. Dillon, J.H. Miller, and K. Omidvar, J. Chem. Phys. **87**, 6967 (1987).
- [27] A. Hamnett, W. Stoll, and C.E. Brion, J. Electron Spectrosc. Relat. Phenom. **8**, 367 (1976).
- [28] C. Backx and M.J. Van der Wiel, J. Phys. B **18**, 3020 (1975).
- [29] L. Vriens, in *Case Studies in Atomic Physics*, edited by E. W. McDaniel and M. R. C. McDowell (North-Holland, Amsterdam, 1969), Vol. 1, p. 335.
- [30] H.C. Straub, P. Renault, B.G. Lindsay, K.A. Smith, and R.F. Stebbings, Phys. Rev. A **54**, 2146 (1996).
- [31] H.C. Straub, B.G. Lindsay, K.A. Smith, and R.F. Stebbings, J. Chem. Phys. **108**, 109 (1998).
- [32] H.C. Straub, B.G. Lindsay, K.A. Smith, and R.F. Stebbings, J. Chem. Phys. **105**, 4015 (1996).
- [33] H.C. Straub, D. Lin, B.G. Lindsay, K.A. Smith, and R.F. Stebbings, J. Chem. Phys. **106**, 4430 (1997).
- [34] D.R. Sieglaff, R. Rejoub, B.G. Lindsay, and R.F. Stebbings, J. Phys. B **34**, 799 (2001).
- [35] B. G. Lindsay and M. A. Mangan, in *Photon- and Electron-Interactions With Molecules: Ionization and Dissociation*, edited by Y. Itikawa, Landolt-Börnstein, New Series, Group 1, Vol. 17, Pt. C (Springer-Verlag, Berlin, in press).
- [36] D. Rapp and P. Englander-Golden, J. Chem. Phys. **43**, 1464 (1965).
- [37] L.G. Christophorou, J.K. Olthoff, and M.V.V.S. Rao, J. Phys. Chem. Ref. Data **25**, 1341 (1996).
- [38] L.G. Christophorou and J.K. Olthoff, J. Phys. Chem. Ref. Data **28**, 967 (2000).
- [39] T.H. Dunning, J. Chem. Phys. **90**, 1007 (1989); R.A. Kendall, T.H. Dunning, and R.J. Harrison, *ibid.* **96**, 6796 (1992).
- [40] P.J. Knowles, C. Hampel, and H.-J. Werner, J. Chem. Phys. **99**, 5219 (1993).
- [41] J.D. Watts, J. Gauss, and R.J. Bartlett, J. Chem. Phys. **98**, 8718 (1993).
- [42] H.-J. Werner and P.J. Knowles, J. Chem. Phys. **89**, 5803 (1988); P.J. Knowles and H.-J. Werner, Chem. Phys. Lett. **145**, 514 (1988).
- [43] MOLPRO is a package of *ab initio* programs written by H.-J. Werner and P. J. Knowles, with contributions from J. Almlöf, *et al.*
- [44] R. D. Levin and S. G. Lias, NBS Report No. NSRDS-NBS 71, 1982 (unpublished).
- [45] D. Margreiter, H. Deutsch, M. Schmidt, and T.D. Märk, Int. J. Mass Spectrom. Ion Processes **100**, 157 (1990).

- [46] C. Backx, G.R. Wright, R.R. Tol, and M.J. Van der Wiel, *J. Phys. B* **8**, 3007 (1975).
- [47] H. Chatham, D. Hills, R. Robertson, and A. Gallagher, *J. Chem. Phys.* **81**, 1770 (1984).
- [48] O.J. Orient and S.K. Srivastava, *J. Phys. B* **20**, 3923 (1987).
- [49] V. Tarnovsky, A. Levin, H. Deutsch, and K. Becker, *J. Phys. B* **29**, 139 (1996).
- [50] B. Adamczyk, A.J.H. Boerboom, B.L. Schram, and J. Kistemaker, *J. Chem. Phys.* **44**, 4640 (1966).